Received: 12 January 2021 | Revised: 21 December 2021 | Accepted: 31 January 2022

DOI: 10.1111/jfr3.12795

ORIGINAL ARTICLE

CIWEM Chartered Institution of Water and Environmental Management | Journal of Flood Risk Management | WILEY

Identification of flood-prone areas with GeoFlood: Lessons learned from the Tiber River case study

Claudia D'Angelo[1] | **Paola Passalacqua**[2] | **Aldo Fiori**[1] | **Elena Volpi**[1]

[1]Department of Engineering, Roma Tre University, Rome, Italy

[2]Department of Civil, Architectural, and Environmental Engineering and Center for Water and the Environment, University of Texas at Austin, Austin, Texas, USA

Correspondence
Elena Volpi, Department of Engineering, Roma Tre University, Rome, Italy.
Email: elena.volpi@uniroma3.it

Funding information
National Oceanic and Atmospheric Administration, Grant/Award Number: NA19OAR4590229

Abstract

Flood mapping is a vital component for sustainable land use in flood-prone areas. Due to the frequency of flood events, local authorities demand effective yet simple methods for the preliminary identification of flood-prone areas at large scales to subsequently define mitigation strategies. We focus here on the workflow GeoFlood, a parsimonious model which uses only high-resolution Digital Terrain Models (DTMs) to define the geomorphological and hydrological information necessary for flood inundation mapping, thus allowing for large-scale simulations at a reasonable computational cost. The purpose of the present study is to investigate the conditions under which GeoFlood is able to correctly reproduce inundation scenarios (with an assigned return period) and their flooding characteristics. Specifically, we analyze its performance over a highly urbanized area, the mid-lower portion of the Tiber River (Italy). We simulated the 200-year return period scenario and compared the results to those provided by the local authority. A sensitivity analysis is performed to quantify the influence of the main geometric and hydraulic parameters involved. Results show that GeoFlood produces rapid flood estimation than can be used in support of standard costly methods over large scales, quickly pointing out the critical flood-prone areas, with consideration of all the uncertainties involved.

KEYWORDS

flood mapping, flood risk, high-resolution terrain analysis, hydraulic modeling, large-scale 2D hydraulic modeling

1 | INTRODUCTION

Floods are one of the most frequent natural disasters in the world and have the potential to cause fatalities, displace people and damage the environment, severely compromise economic development, and undermine economic activities (EU Floods Directive, 2007/60/EC). Hence, local authorities are required to assess flood hazard conditions in order to prevent damage and plan mitigation strategies. Further, several warning services, such as emergency plans, dissemination, etc., are usually developed to enhance awareness in areas that might be affected by flooding such that emergency response can be effective (Ball et al., 2012). Due to the frequent and sparse occurrence of intense and not so predictable events and to the huge consequences that those events might produce, a

preliminary assessment of large-scale flood preparedness for emergency response is mandatory.

Inundation maps lie at the base of flood risk management, providing fundamental information for both land use planning and flood emergency response (Apel et al., 2009; van Alphen et al., 2009). Modeling approaches for flood mapping involve several steps, from the statistical analysis to estimate the probability of occurrence (or return period) of flow discharge, to the hydraulic simulation that is required to estimate flood extent, water surface elevation, and velocity over the inundated area. Depending on the final goal, the hazard analysis can be performed at different scales, but as a consequence of the complexity of the processes involved and the simplifications introduced by the models, flood mapping and risk analysis are generally characterized by a large degree of uncertainty (Annis, Nardi, Volpi, & Fiori, 2020; Apel et al., 2004, 2008; Bales & Wagner, 2009). Further, they might be biased since these models largely ignore basic interactions and feedbacks among atmospheric processes, catchment and river-floodplain characteristics, and socioeconomic processes (Vorogushyn et al., 2018).

The approaches used for flood inundation mapping can be divided into three main categories (Teng et al., 2017): (i) empirical methods, based exclusively on the analysis of observations, (ii) simplified conceptual models, which add to purely empirical methods by including simplified hydraulic concepts, and (iii) hydrodynamic models, solving equations formulated by applying the laws of physics, that is, one-dimensional Saint-Venant equations, two-dimensional shallow water equations, etc.

Purely DTM-based methods (i) allow the identification of areas that are geomorphologically prone to inundation (most recent works: Manfreda et al., 2011, 2014; Samela et al., 2016, 2018; Annis & Nardi, 2021), without performing any hydraulic simulation. For this reason, these methods do not require any discharge estimation as input to the model. They are generally suited for application to large areas, real-time monitoring, and post-event evaluation. Indeed, the advantages offered by these geomorphological models are their parsimony in terms of required information (only a DTM) and the decreased computational time with respect to hydrodynamic models (Annis et al., 2019; Di Baldassarre et al., 2020).

Results produced with these models are strongly affected by the spatial resolution of the input data (Horrit & Bates, 2001; Savage et al., 2016); hence, new approaches have been developed which are capable of mapping large geographic areas at high resolution (Annis et al., 2019; Di Baldassarre et al., 2020; Manfreda & Samela, 2019). It is important to stress that the resolution of the DTM does not impact only the estimation of water heights through flood mapping, it also affects the representation of property exposure and, correspondingly, the accuracy of flood damage and risk estimation (Komolafe et al., 2018). To those aims, high-resolution LIDAR-derived DTMs are preferable, since they introduce more detailed information, including basin hydrogeomorphic behavior (Annis, Nardi, Petroselli, et al., 2020; Petroselli, 2012). Obviously, this information is lost when resampling the LIDAR-derived DTM to a coarse resolution for running large-scale models (Savage et al., 2016).

Notwithstanding the improvement derived by the use of detailed topographic information, the use of purely DTM-based methods for flood preparedness is limited. Indeed, flood maps resulting from these approaches cannot be easily characterized in terms of expected frequency of occurrence (i.e., return period scenarios), which is mandatory for risk assessment and land use planning purposes.

Simplified conceptual approaches (ii) overcome the above limitation by allowing for variable flood level as a function of the return period. Among them, we recall the Rapid Flood Spreading Method (RFSM) (Lhomme et al., 2008), the planar or bathtub method (Teng et al., 2015), the Height Above Nearest Drainage (HAND) approach (Nobre et al., 2011), and the hydrogeomorphic approach by Nardi et al. (2006). Simplified conceptual approaches rely primarily on a DTM dataset, yet not only. They provide also useful information for emergency response application by requiring significantly less computer effort than the hydrodynamic models. Performing simulations during emergencies usually requires a hydrologic input; when available, the uncertainty characterizing the hydrologic input is expected to overwhelm that due to approximate hydraulic computations, thus strengthening the choice of simplified modeling strategies (Annis & Nardi, 2021).

Hydrodynamic modeling (iii) is the most widely used method in flood extent mapping and risk estimation studies. Its use at a high resolution is especially suited to local scale analysis, being able to provide distributed information of time-varying water level and velocity in the inundated areas for any return period scenario, at a usually high economic and computational cost. Hydrodynamic simulations are also performed for large-scale analysis at medium to low resolution, providing acceptable results at a reasonable computational cost (see, e.g., Bates et al., 2021 and references therein). Note, however, that 1D or 2D hydrodynamic modeling typically requires: time-varying flow discharge for the return period of interest; detailed geomorphological and hydraulic information based on local surveys, including those pertaining to the structures and infrastructures that might affect flow

propagation; detailed terrain representation, and land use and characteristics of the urban settlements of the areas potentially inundated. The reader is referred to Teng et al. (2017) for a review of the methods and a list of software/models available in the literature, with special focus on 2D models.

The choice of the method to be used for flood inundation mapping is based on finding a good compromise between inundation maps accuracy and modeling cost, taking into account the large degree of uncertainty that characterizes the estimated results. Specifically, it should be considered that the overall estimation uncertainty is dominated by the uncertainty in flow discharge quantification, which overwhelms that due to hydraulic modeling under general conditions (see Annis, Nardi, et al., 2020, and references therein).

In applications to large areas, the computational effort required by hydrodynamic modeling might be reduced by omitting certain terms in the equations to be solved, resulting in diffusive or kinematic wave approximations. Further simplifications, providing consistent inundation simulations with shorter running times, are obtained by neglecting the local effects of infrastructures (Arrighi & Campo, 2019; Bales & Wagner, 2009; Koivumaki et al., 2010) and by adopting a coarse spatial resolution (Alfieri et al., 2014; Dottori et al., 2016; Pappenberger et al., 2012; Pena & Nardi, 2018; Sampson et al., 2015; Schumann et al., 2013; Wing et al., 2017; Winsemius et al., 2013). The latter simplification might be avoided to some extent by allowing for multi-core processing that is able to model large areas without having to make strong compromises regarding spatial detail (Tyrna et al., 2018).

A promising solution in this direction was recently proposed by Zheng, Maidment, et al. (2018); Zheng, Tarboton, et al. (2018). The authors presented GeoFlood, a simplified modeling approach that makes use of a high-resolution topographic dataset (LIDAR-derived DTM) for the definition of geomorphic and hydraulic features. Channel extraction and the definition of the hydraulic parameters (stage-discharge relationship) are implemented through the analysis of the DTM and the Height Above Nearest Drainage (HAND) raster (Nobre et al., 2011), which makes GeoFlood a parsimonious model. The simplifications listed above allow reducing the overall modeling cost with respect to a "standard" hydrodynamic detailed solution; but a reduction in accuracy of the resulting flood extents and depths might be expected.

The main purpose of this study is to investigate the conditions under which the large-scale simplified flood model GeoFlood (Zheng, Maidment, et al., 2018; Zheng, Tarboton, et al., 2018) is able to correctly reproduce inundation scenarios in terms of extent and depth. To this aim, we present and discuss the application of this approach to the medium-lower portion of the River Tiber (Italy). We produce flood maps for a 200-year return period scenario and compare them to the maps produced by the local authority by using standard resources based on local modeling. We perform a sensitivity analysis by providing a quantitative evaluation of the influence of DTM resolution, channel segmentation length, and Manning's roughness coefficient.

The article is organized as follows. In Section 2, we briefly describe the workflow GeoFlood. In Section 3, the case study and the data available for the analyses are presented. In Section 4, we illustrate the results of our analyses in terms of inundation extent, cross-sectional inundation extent, and water level profiles. A discussion of the results and recommendations for future applications are provided in Section 5. The main conclusions drawn from our study are summarized in Section 6.

2 | OVERVIEW OF THE WORKFLOW GEOFLOOD

The workflow GeoFlood can rapidly convert river flow conditions to corresponding flood maps at a large scale, from high-resolution topographic data and at low computational cost (Zheng, Maidment, et al., 2018; Zheng, Tarboton, et al., 2018). To create inundation maps, GeoFlood only requires topography, as represented by a DTM, and distributed information of the peak flow discharge over the entire river network.

GeoFlood computes flood inundation extent and depth under uniform conditions along river segments, including channel and floodplains and delineated from flow directions, by combining two methods, GeoNet and Height Above Nearest Drainage (HAND). GeoNet is an automatic tool for geomorphic feature extraction from high-resolution topographic data (Passalacqua et al., 2010; Sangireddy et al., 2016). A HAND raster quantifies the elevation difference between each land surface cell and the stream bed cell to which it drains (Nobre et al., 2011, 2015), using the network extracted from high-resolution terrain data. This elevation difference represents the water level value at which that cell will be inundated. The procedure for inundation map delineation based on the Geoflood workflow is described below.

The channel network is extracted from the DTM following the GeoNet procedure. The channel extraction process comprises three major operations: non-linear filtering of the elevation data, identification of the likely channelized pixels based on curvature and accumulation area computed on the filtered DTM, and a least-cost-path

approach for channel network identification based on terrain curvature and flow accumulation area.

GeoNet may constrain the network to pass through some a-priori known nodes, when available. This allows to have a very good planar correspondence between the extracted river network and the one a-priori known, so that the problem of flood input attribution in specific river sections (as explained below) becomes negligible. Planar discrepancies are further reduced if a conditional DTM is used, that is a DTM corrected for to properly represent terrain elevation in the main channel.

Within GeoFlood, the river network is divided into equal-length parts, denoted as segments (Godbout et al., 2019). Segment length is one of the framework parameters that affects the performance of the method.

For each segment, analyzed individually, a synthetic rating curve is produced (Zheng, Maidment, et al., 2018; Zheng, Tarboton, et al., 2018). This is done by extracting the water surface extent, bed area, and flooded volume as function of the water level for each of the segments. The evaluation of those hydraulic quantities is based on the HAND method, that is, taking into account the flow directions and without making any distinction between channel and floodplains, which means that both contribute to the rating curve at water levels above bankfull. Dividing the water surface extent, bed area, and flood volume by the associated segment length, all the hydraulic parameters ruling the stage-discharge relationships can be derived, namely the top width, cross-sectional wetted area, wetted perimeter and eventually the hydraulic radius. Note that the resolution of the DTM plays an important role also in this step of the analysis because the path of the extracted feature is strongly influenced by the terrain detailed characteristics.

The workflow does not use cross-sections, extracted from the DTM or provided from external sources, yet it is based on averaging the hydraulic quantities to define a cross-section that might be assumed constant over the entire segment. The discharge depends on water level through the Manning roughness coefficient, which is another relevant parameter (Godbout et al., 2019).

In order to delineate a flood map, an input discharge needs to be provided from an external source as peak flow distributed along the river network, while no flow levels are necessary to perform the hydraulic simulation. Note indeed that the simulation is performed under uniform conditions, so that the water level can be computed in each segment once the peak discharge is known. Peak flow values known in specific river sections are attributed to the same sections in the channel network as extracted by GeoNet and assumed to be constant over river segments. If peak flow values are not available for each river segment identified by the analyst, they can be, for example, linearly interpolated.

Over each segment, the peak flow input is converted into a depth through the rating curve. Finally, the water depth is distributed over the catchment using again the HAND method, that is, accounting for flow paths, resulting in the delineation of the inundated areas.

3 | CASE STUDY: THE TIBER RIVER

The Tiber River is one of the largest river basins in Italy, flowing from the Apennine Mountains to the Tyrrhenian Sea. It runs through several regions that are Emilia-Romagna, Marche, Toscana, Umbria, Abruzzo, and Lazio, draining the city of Rome. Along its course, it runs through several towns and cities providing economic and agricultural benefits. As a result, strategic infrastructures such as road and rail arteries that connect the entire peninsula are developed within its domain. The dominant land use for the basin is agriculture, covering about 53% of the surface, while approximately 39% is forested and 5% is urbanized, as reported by the Tiber River Basin Authority (TRBA). Considering the flood adverse impacts in this particular area, the Tiber has been frequently investigated to define flood risk conditions and identify the appropriate mitigation strategies for land protection. Specifically, accurate analyses related to return period scenarios, as also indicated by the EU Flood Directive (2007/60), are crucial for the design of new hydraulic infrastructures and the assessment of structures already present.

The Tiber drains an area of approximately 17,500 km^2 and it is 406 km long. We focus on the medium-lower portion for a total length of 168 km, from Corbara dam to the Castel Giubileo small dam, (Figure 1, red line). This river stretch is characterized by a succession of gorges and broad valleys that strongly influences the river regime in the city of Rome. In this part of the river, flood events negatively affect the economy of the entire area. The three main infrastructures that regulate the flow in this area are Alviano, Ponte Felice, and Nazzano small dams, located at a distance of about 20, 60, and 120 km from Corbara dam, respectively.

We followed the procedure presented in the previous section to generate 200-year inundation maps of the medium-lower portion of the Tiber River. The GeoFlood results are compared with the flood maps provided by the Central Apennine Hydrographic District, the authority of which the TRBA is part of since 2006. Following the Flood Risk Management Plan (under the Italian Law 49/2010), PAI flood maps ("Piano di Assetto Idrogeologico", which may be translated as Hydrogeologic Risk Plan) have been revised and standardized by the Central Apennine Hydrographic District

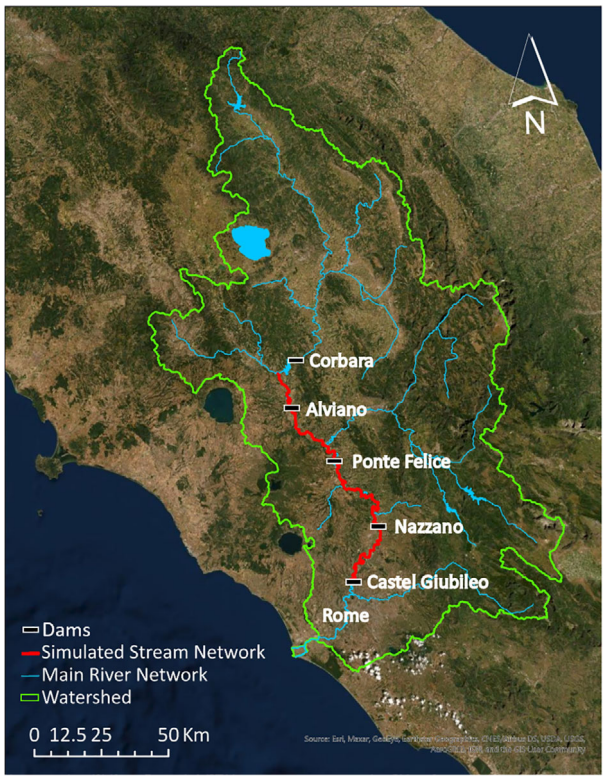

FIGURE 1 River Tiber watershed (17.375 km^2). The stream network simulated with the workflow GeoFlood is part of the medium-lower portion of the watershed of 168 km length, from the Corbara dam to Castel Giubileo small dam. The analyzed watercourse is characterized by the presence of three small dams: Alviano, Ponte Felice and Nazzano

producing prediction maps where the flood is classified in terms of hazard. Maps are derived from hydrodynamic modeling, HEC-RAS (USACE, 2016) and FRESCURE, with a 4 × 4 m DTM as input. Maps have been published in 2013 in the PGRAAC ("Piano di Gestione del Rischio Alluvioni dell'Appennino Centrale", that is the management plan of flood risk of the Central Apennine).

The input data for the present study are: 2-meter Lidar-derived DTM available for the river zone produced by the Italian Ministry of the Environment, used for geomorphological analysis at different spatial resolutions (as detailed in the following section); Manning's roughness coefficients for the channel ($n_c = 0.037$ s/m$^{1/3}$) and the floodplain area ($n_f = 0.08$ s/m$^{1/3}$) provided by the PGRAAC, used for rating curve estimation; 200-year return period discharge peak flow values and the corresponding water levels for every cross section along the selected area provided by the PGRAAC, used for inundation maps delineation and assessment, respectively.

Note that the DTM used here was preliminarily conditioned in order to correctly reproduce the channel bed elevation, otherwise influenced by the presence of water. The latter might have negligible effects, yet not in the case analyzed here due to the presence of small dams. Indeed, the channel slope reproduced by the raw DTM was too small right upstream of the dams and almost correct far from them.

4 | RESULTS

In the following we show the GeoFlood results obtained performing a sensitivity analysis of this set of conditions: DTM resolution (2 × 2 m, 4 × 4 m, 8 × 8 m, 16 × 16 m); channel segment length ($L = 2$ km, $L = 5$ km, $L = 10$ km); Manning's roughness coefficients (PGRAAC averaged $\overline{n}$ as defined later on, PGRAAC n_c and n_f which are the minimum and maximum n values for the channel and the floodplain, respectively). The DTM at different resolutions is used in the entire procedure as described in Section 2, that is, from geomorphological analysis (i.e., river network extraction) to map delineation. Channel segment length and Manning coefficient values influence the rating curve of each segment and the inundation delineation.

We compare the results in terms of flooded area, cross-sectional inundation extent, and water levels using the PGRAAC data as benchmark. For the inundation extent comparison, we converted the flooded area in the PGRAAC map into a raster layer, with a resulting area $A_{\mathrm{TRBA}} = 144.42$ km^2. The comparison is made by overlapping raster layers from each simulation to point out over- and under-estimation of the flood extent obtained from GeoFlood with respect to the PGRAAC layer. Figure 2 shows the comparison of the inundation extent produced with GeoFlood and the PGRAAC map for the whole region; in the figure, the simulation is performed with the 2 × 2 m DTM, river segmentation length $L = 5$ km, and Manning coefficient equal to $\overline{n}$. The GeoFlood inundated area is equal to $A = 152.32$ km^2. In the following, results in terms of inundation extent are shown in subsets of the entire map (bounded by black boxes in Figure 2) to better highlight the details of the results.

To quantify the comparison, we used the area ratio between GeoFlood results (A) and the PGRAAC layer (A_{TRBA}), defined as $r_A = A/A_{\mathrm{TRBA}}$.

To highlight local differences in terms of flood extent, we selected 40 river cross-sections (not shown in the maps for the sake of clarity) from the PGRAAC map to show the cross-sectional inundation extent for each set of simulations, offering a numerical quantification of the local differences. The comparison is made by measuring the flooded width produced with GeoFlood in locations where the PGRAAC has information about cross-sections. We also evaluated the standard deviation of the

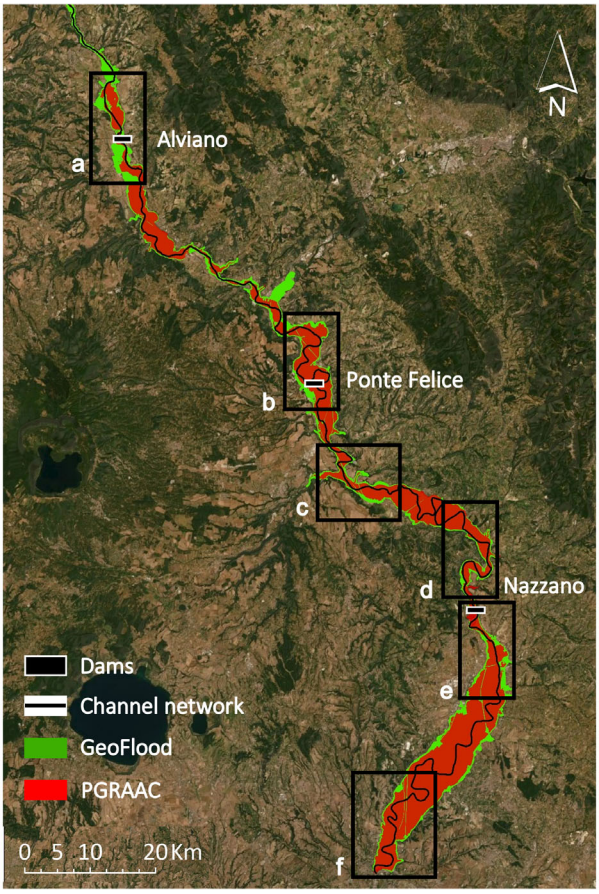

FIGURE 2 Comparison of the inundation extent performed with GeoFlood considering 2 × 2 m DTM resolutions, river segmentation length $L = 5$ km and a manning coefficient equal to n, and the flooding produced by the river authorities for the whole area. Alviano, Ponte Felice and Nazzano small dams, are reported on the figure as well

ratio between the GeoFlood and PGRAAC inundation extents, its maximum and minimum values, and an absolute value of the discrepancy with the PGRAAC for each curve, defined as the percentage of cross-sections where the mismatch is larger than 500 m.

Regarding the water level profile, the results of any GeoFlood simulations are produced by adding the stream bed elevation from the DTM to the depths obtained from the synthetic rating curves. The root mean square error σ_w (m) between the water level profiles is used to quantitatively compare results.

In the following, we show the results of the sensitivity analysis for each of the relevant parameter.

4.1 | DTM resolution

The inundation extent produced by varying the DTM resolution is performed considering $L = 5$ km channel segments and the PGRAAC average Manning value $\overline{n}$. The DTM resolution influences the channel network extraction, thus for each simulation we obtain a different path and, as a consequence, a different channel slope that might produce a different flood extent. However, there is not a big difference among the results, especially in most of the river portions (Figure 3). Nevertheless, there is a slight over-estimation, which is noticeable in all the simulations specifically close to the Alviano small dam (panel a, Figure 3). PGRAAC flood area is equal to 144.42 km^2, while the GeoFlood inundated area is equal to 152.32, 149.82, 152.32, and 152.62 km^2 for the 2 × 2, 4 × 4, 8 × 8, and 16 × 16 DTM resolutions, respectively.

The area ratio for each resolution is: $r_A = 1.05$ for 2 × 2 m DTM (green layer); $r_A = 1.04$ for 4 × 4 m DTM (dark-green layer); $r_A = 1.05$ for 8 × 8 m DTM (cyan layer); $r_A = 1.06$ for 16 × 16 m DTM (light-blue layer). In general, it emerges that the coarser is the DTM resolution, the stronger is the over-estimation of the inundation extent from the model; indeed, coarser resolutions provide a more regular pattern of the terrain, so that terrain variability is removed and water flows smoothly. This is true except at locations where characteristics of the terrain or the river affected by grid resolution might influence the area ratio. For example, the underestimation of the inundated area that is visible in the upper part of Figure 3d is due to the misrepresentation of the river meander at the resolutions of 4 × 4 m and 8 × 8 m.

This underestimation is clearly visible also in Figure 4 in terms of cross-sectional inundation extent. Figure 4 shows the cross-sectional inundation extent by varying DTM resolution; each series refers to the inundation extents shown in Figure 3 and is depicted with the corresponding raster layer's color. The series of gorges and valleys typical of our study area are clearly visible, with valleys located at a distance of 60 km (see panel b of Figure 3), 90 km (between panels c and d), and 130 km (between panels e and f). All the performed simulations tend to fit well the PGRAAC curve with a slight over-estimation of the flood extent, even if there are exceptions at local scales. The over-estimation is mainly focused in the first 20 km from upstream and at a distance of 50, 90, and 130 km. The percentage of large error in cross sections (mismatch larger than 500 m) is generally increasing from about 10% to about 25% when reducing the resolution of the DTM from 2 × 2 to 16 × 16 m.

Figure 5 shows the results in terms of water level. Apart from local differences, the GeoFlood water profiles closely follow the reference one. Local differences and the irregular stepped behavior are due to the nature of the simplified hydraulic modeling approach used in GeoFlood; indeed, each segment is resolved

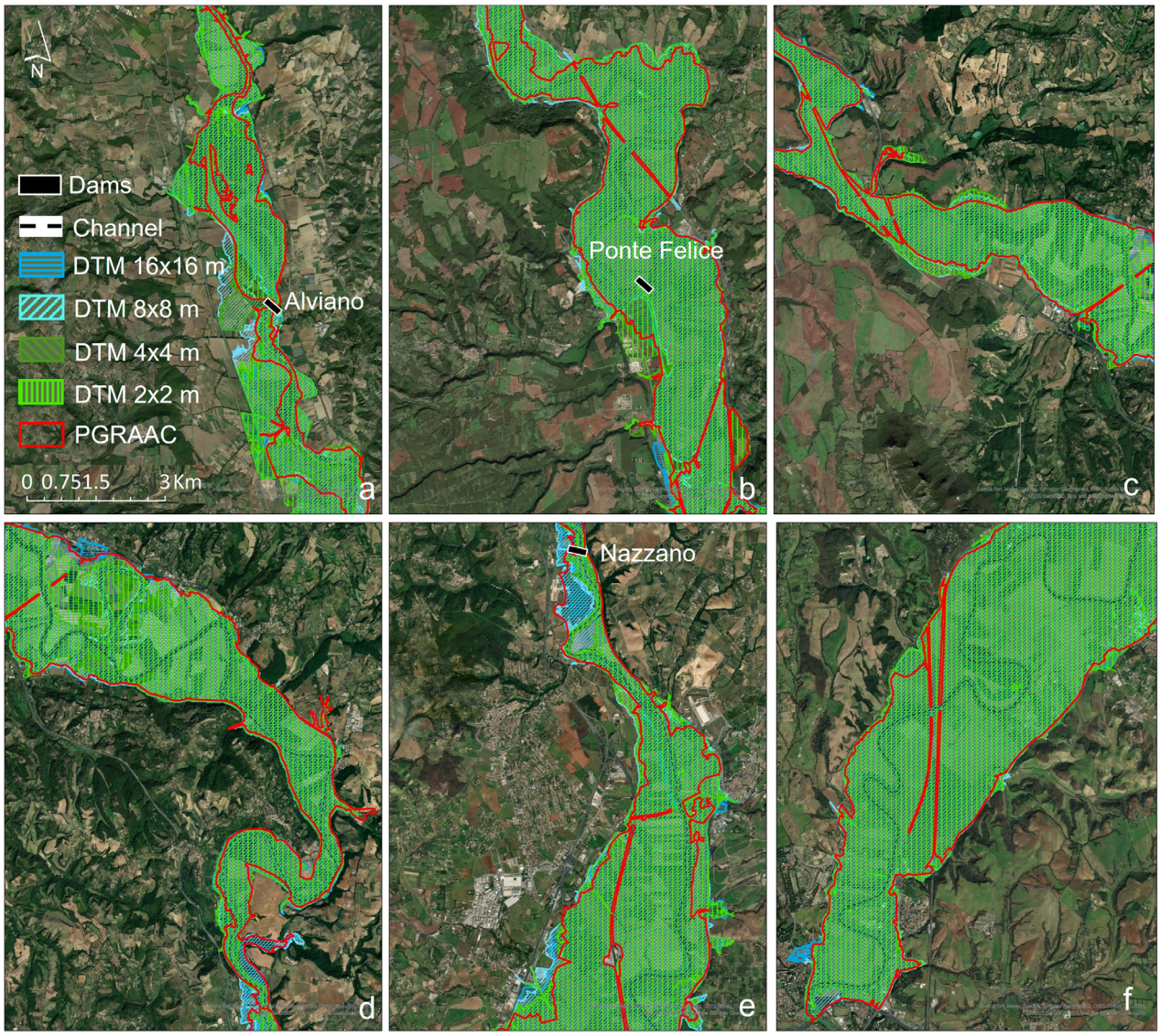

FIGURE 3 Comparison of the inundation extent performed with GeoFlood considering different DTM resolutions, river segmentation length $L = 5$ km and a Manning coefficient equal to n, and the flooding produced by the river authorities; the six portions of the medium-lower Tiber River valley are highlighted in Figure 2. The most important hydraulic structures along the river, that are Alviano, Ponte Felice and Nazzano small dams, are reported on the figure as well

independently from up- and downstream ones, under uniform conditions. The water level in each segment is mainly controlled by the riverbed slope, through the stage-discharge relationship; as an example, due to the main channel steepness downstream the Nazzano small dam, we have a water level smaller than the PGRAAC one, which is influenced by downstream conditions (see Figures 3e, 4, and 5). This behavior emerges for high DTM resolution, while it is attenuated when the resolution is lowered.

The irregular behavior of the water profiles is also partially determined by the location and elevation of the channel extracted, and consequently by the DTM resolution, as shown in Figure 5. Indeed, the extracted channel is different for each resolution, showing also a shift at the distance of about 90 km, in essence due to the misrepresentation of the river meander for DTM resolutions of 4×4 and 8×8 m. The root mean square error for each scenario is $\sigma_w = 3.0$ m for 2×2 m DTM, $\sigma_w = 4.0$ m for 4×4 m DTM, $\sigma_w = 2.9$ m for 8×8 m DTM, and $\sigma_w = 3.5$ m for 16×16 m DTM, respectively. Lowering the resolution of the DTM results in an attenuation of the irregular behavior and a slight increase of the overall over-estimation.

Finally, the presence of small dams and other infrastructures like bridges, represented as vertical dashed lines in Figure 5 and not explicitly accounted for by GeoFlood, do not have any effect on the results. As

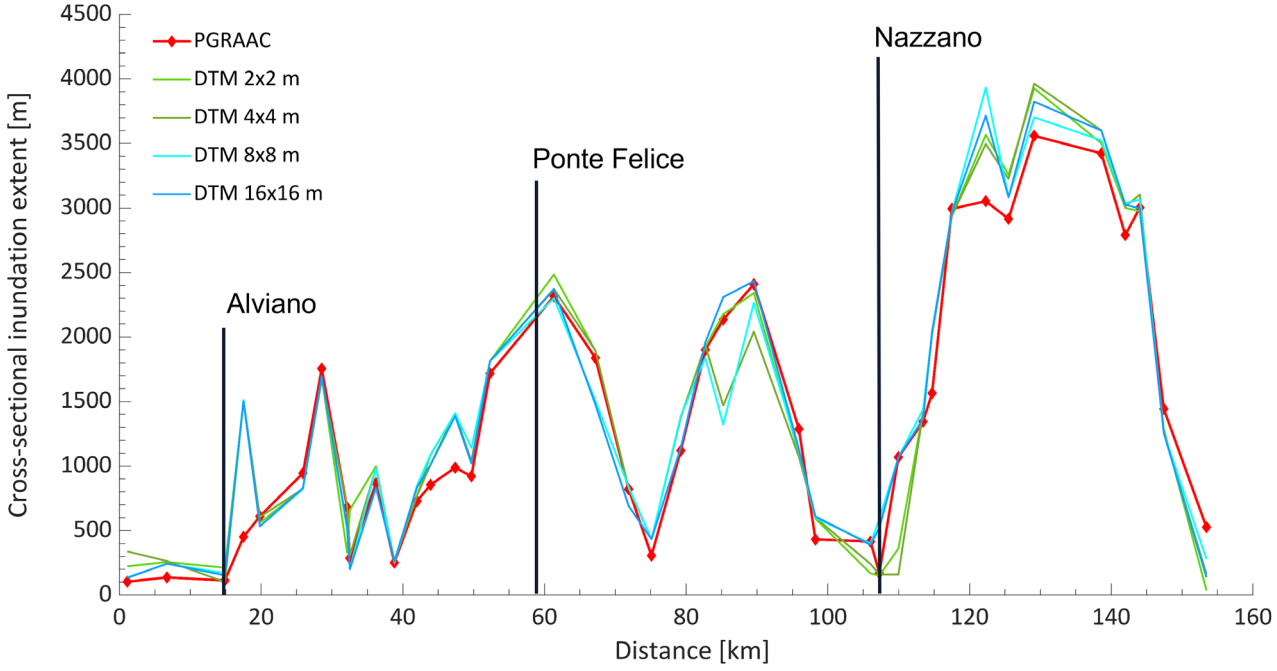

FIGURE 4 Cross-sectional inundation extent for 40 cross sections along the extracted network for different DTM resolution, as in Figure 3. Cross sections position is identified with diamonds on the red curve

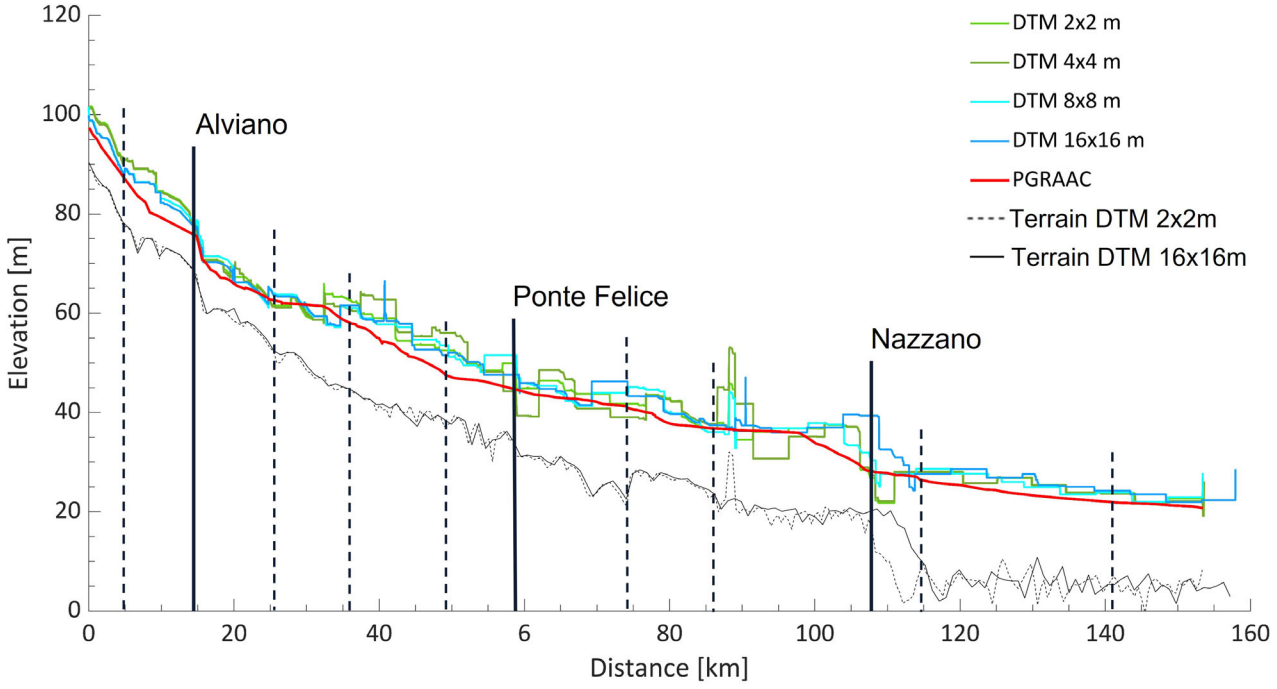

FIGURE 5 Water level profile for the entire length of the simulated river portion for different DTM resolutions, $L = 5$ km segment and n Manning coefficient. The location of the small dams is depicted with black lines, black-dashed vertical lines represent the location of the main bridges

mentioned in Section 3, our study area is highly urbanized, with many highways and railways crossing the Tiber River course; notwithstanding, there is no evidence in the PGRAAC profile of their presence.

4.2 | Channel segment length

The channel segment length is a crucial parameter that can significantly influence the results. To investigate the

relevance of this parameter, we performed several simulations with different channel segmentation lengths at the higher-resolution DTM (2 × 2 m) and Manning coefficient $\overline{n}$.

Overall, we noticed a slight over-estimation in the order of 5% of the flood extent, apart from the case of $L = 2$ km (Figure 6). In terms of area ratio, we found $r_A = 0.97$ for a 2 km long segment (orange layer), $r_A = 1.05$ for a 5 km long segment (green layer) and $r_A = 1.04$ for a 10 km long segment (blue layer). The flooded area is 140.02, 152.32, and 149.53 km^2 for $L = 2.5$ and 10 km, respectively.

For $L = 2$ km, we observe an under-estimation at the river meander (panel d) and downstream the Nazzano small dam that balances the over-estimation (see panel a, upstream Alviano, and panel b, upstream Ponte Felice). Increasing the channel length, we do not observe local under-estimations, apart from right downstream the Nazzano small dams. The same behavior emerges also in terms of cross-sectional inundation extent; the latter is depicted in Figure 7 as function of the distance along the main channel from upstream, and for the three different values of segment length considered in the analysis. In the figure, we can observe for each simulation a tendency to fit the PGRAAC curve, yet with an over-estimation in the first 20 km from upstream and at a distance of 50 and 130 km (as in Figure 4). The percentage of large error in cross sections is about 10% for $L = 2$ and 5 km, while it increases to 20% for $L = 10$ km.

Finally, when we analyze the results in terms of water level profile, the profile for $L = 5$ km is more similar to the one from the PGRAAC with respect to the others

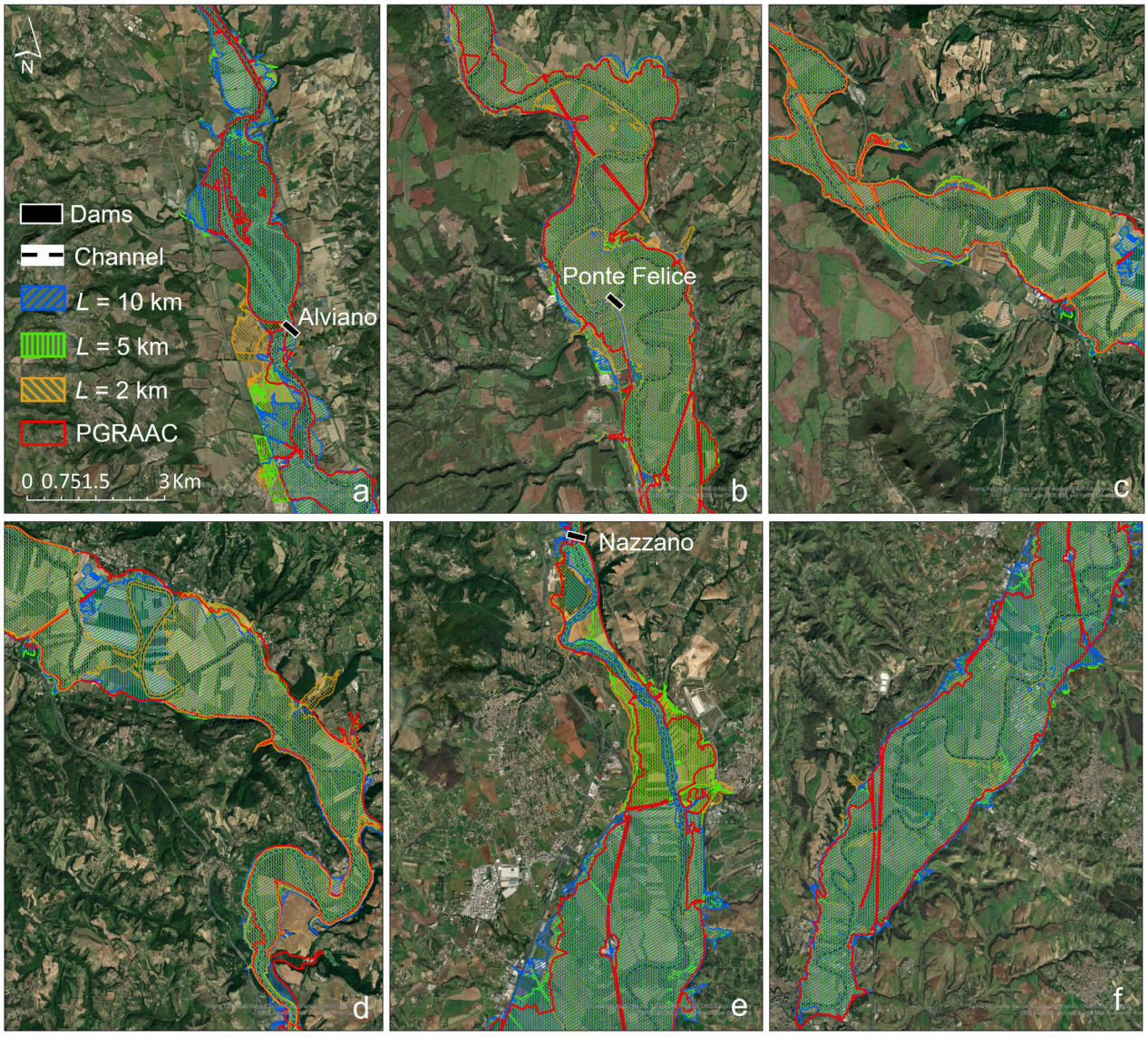

FIGURE 6 Comparison of the inundation extent performed with GeoFlood with different length values L for the channel segments, using a 2 m DTM and a Manning coefficient equal to n, and the flooding extent produced by the river authorities

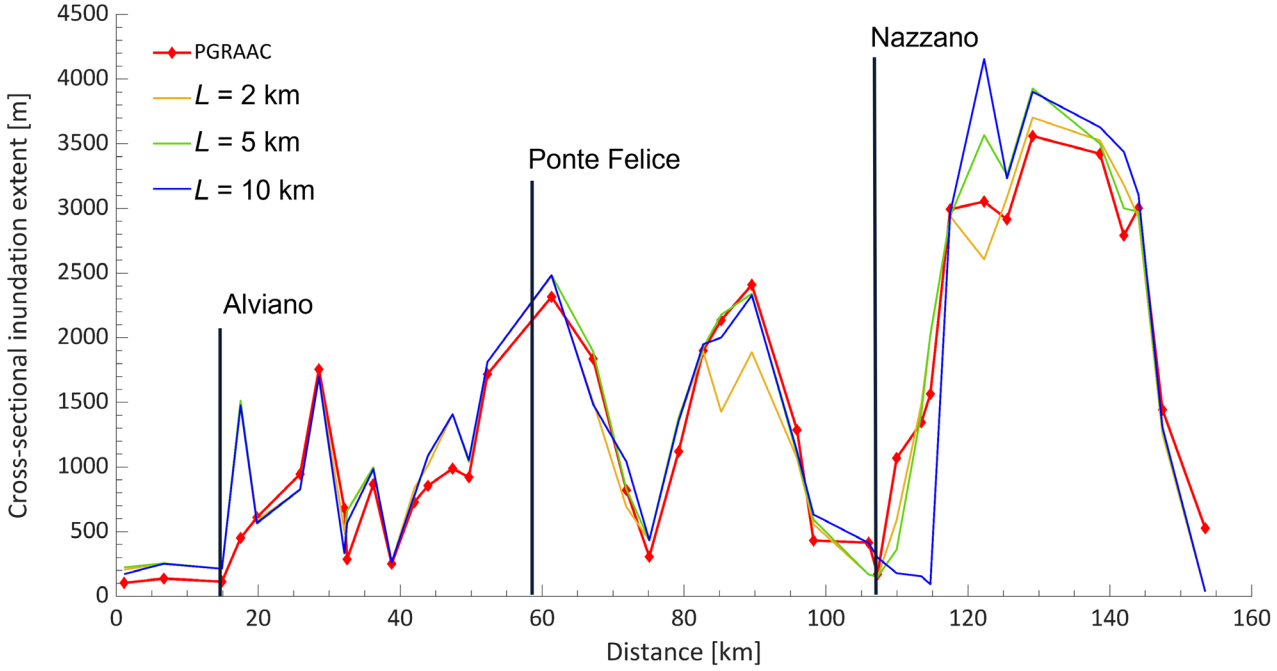

FIGURE 7 Cross-sectional inundation extent for 40 cross sections along the extracted network for different channel segment length L and 2-m DTM resolution. Cross sections position is identified with the diamonds on the red curve

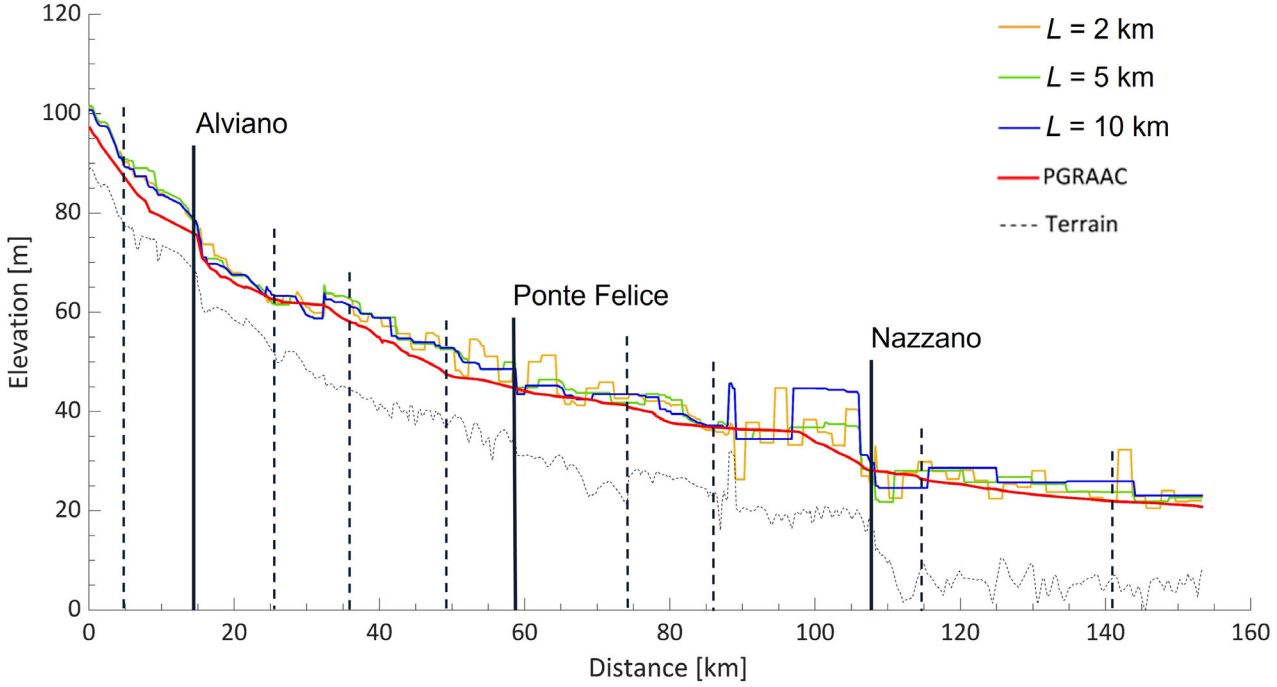

FIGURE 8 Water level profile for different length L of the segments, 2 × 2 m DTM resolution, and n Manning coefficient. The terrain profile represents the elevation of the channel network extracted with the tool GeoNet from a 2 × 2 m DTM resolution. The location of the small dams is depicted with black lines, black-dashed vertical lines represent the location of the main bridges

(Figure 8). The root mean square error is $\sigma_w = 3.0$ m, lower than the other two scenarios, $\sigma_w = 3.7$ m and $\sigma_w = 3.8$ m for 2 and 10 km segment length, respectively. Since GeoFlood assumes constant parameters for the definition of rating curves on each segment, a short segment length generally produces good approximation of local

conditions on average. On the other hand, short segment lengths yield stronger variability in terms of water level, affecting the overall performance of the model (Figure 8 and root mean square error). The opposite happens in the case of long segment length. As a matter of fact, an optimum in channel segmentation length can be identified; the condition that best suits the benchmark in terms of water level for this case study is the 5 km segment.

4.3 | Manning's roughness coefficient

The Manning's roughness coefficient (n) strongly affects the rating curves; the larger the Manning coefficient, the higher the water level in each segment individually. The PGRAAC provides the roughness coefficient for the main channel, $n_c = 0.037\ \mathrm{s/m^{1/3}}$ and the flood-plain area, $n_f = 0.08\ \mathrm{s/m^{1/3}}$. Hence, we first applied GeoFlood considering each n value separately over the whole domain, while the simulations presented in the previous subsections, were performed with an average value based on the cross-sectional extent of channel and floodplain, respectively. Due to the presence of broad valleys, these average values tend to be tightly similar to the floodplain value. This explains the flood extents in Figure 9, where the inundated area obtained with using only the floodplain n_f value is overlapped with the one obtained with averaged values, producing an area ratio $r_A = 1.06$ (purple layer). Since we are simulating a 200-year scenario, the roughness coefficient of the floodplain is expected to have a significant effect. Instead, the minimum value n_c produces a small under-estimation of the flooding extent

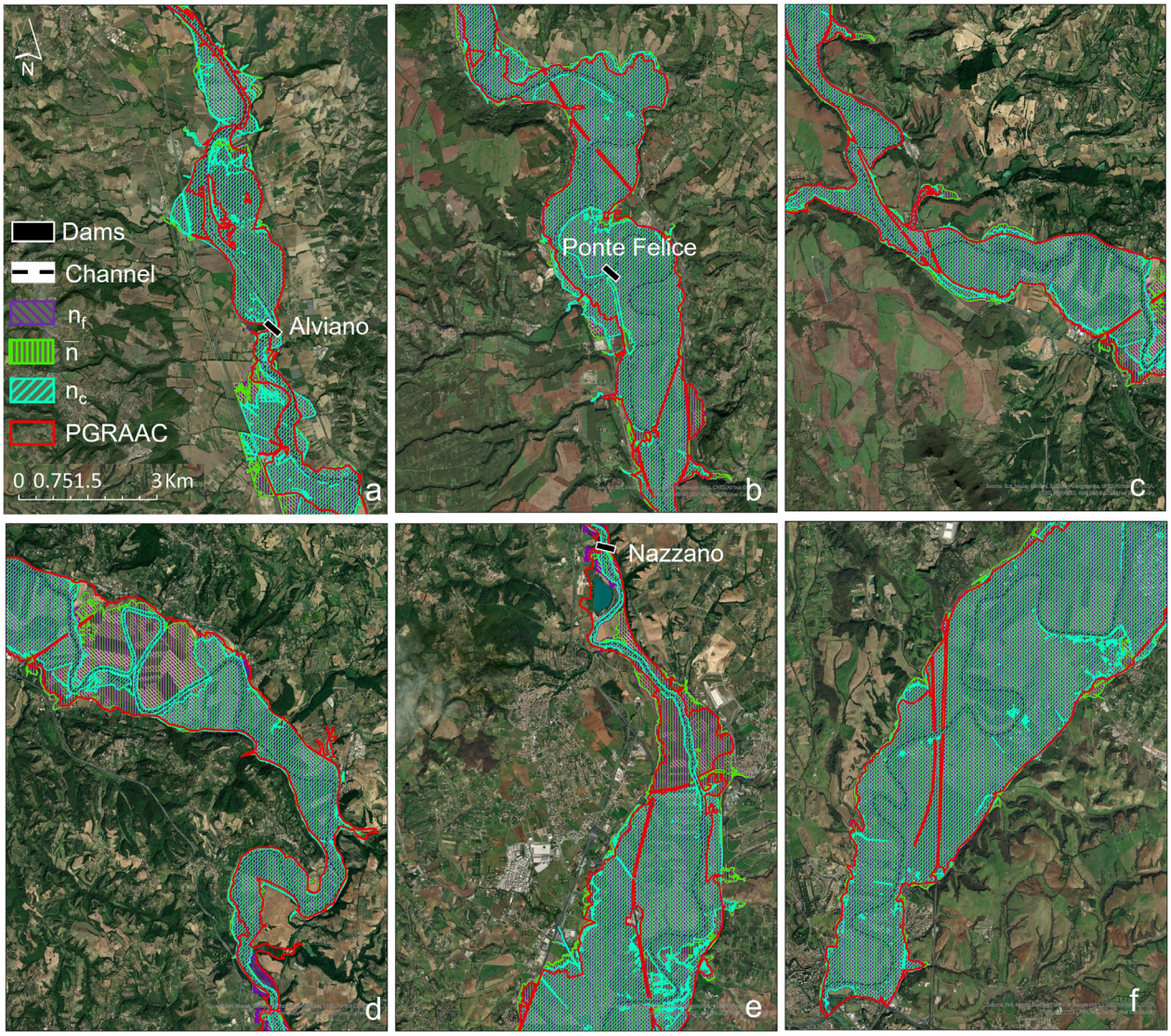

FIGURE 9 Comparison of the inundation extent performed with GeoFlood considering different Manning values n for the channel segments using a 2 DTM and $L = 5$ km as segment length, and the flooding produced by the river authorities

in some critical portions, resulting in an area ratio $r_A = 0.89$ (green water layer). For the maximum value of the Manning coefficient n_f, the flooded area is 153.62 km^2, while for the minimum Manning value it is 128.52 km^2.

Figure 10 shows the results obtained in terms of the cross-sectional inundation extent. In this analysis, we noticed a better match with the PGRAAC result, with the over-estimation similar to Figures 4 and 7, but the under-estimation is also found at several distances. In fact, the minimum error occurs for the simulation performed with the roughness coefficient of the channel $n_c = 0.037$ s/m$^{1/3}$; while the variability of percentage with a mismatch larger than 500 m is less affected by Manning's coefficient, remaining between 10% and 15%.

In terms of water level profile, the simulation with the minimum coefficient value (n_c), generates a better match with the PGRAAC result with a root mean square error of $\sigma_w = 2.2$ m (Figure 11) compared with $\sigma_w = 3.2$ m and $\sigma_w = 3.0$ m pertaining to n_f and $\overline{n}$, respectively. Indeed, the profile corresponding to n_c is closer to that of the PGRAAC simulations, apart from the portion of the river soon after the Nazzano small dam. However, this assumption appears to be inconsistent for a 200-year scenario, where a wider inundation is expected, while the maximum value of the roughness coefficient, n_f, produced a better result with respect to the inundation extent in Figure 5 due to the predominance of the floodplain coefficient in the average $\overline{n}$ value.

5 | DISCUSSION AND RECOMMENDATIONS

The DTM resolution plays a crucial role as it affects the identification of the river network; (see Figure 5 where the riverbed elevation obtained with two different DTM resolutions is depicted). Note, however, that the latter can be significantly affected by other characteristics of the DTM, such as the land use of the area (e.g., urbanized, rural). Regarding our case study, when the resolution is decreased, the terrain becomes more regular; and a coarser resolution implies smaller computational times. However, a coarser resolution facilitates flow propagation yielding a general over-estimation that increases with DTM cell size. This result depends on the morphology of the area, which affects the channel extraction, and the same result is not necessarily expected at all sites. In a highly urbanized area as the one here studied, it may be helpful to constrain the channel extraction operation to 85information. For example, using a conditioned DTM could avoid errors in channel extraction due to the presence of infrastructures (Manfreda et al., 2014), as in the case of the Tiber River.

Indeed, the portion of the Tiber River analyzed in this study is characterized by many existing infrastructures and urban settlements, entailing possible difficulties for the modeling part, at high-resolution specifically. The identification of the valley corridor and the inundation extent resulted rather accurate also in the study by Nardi

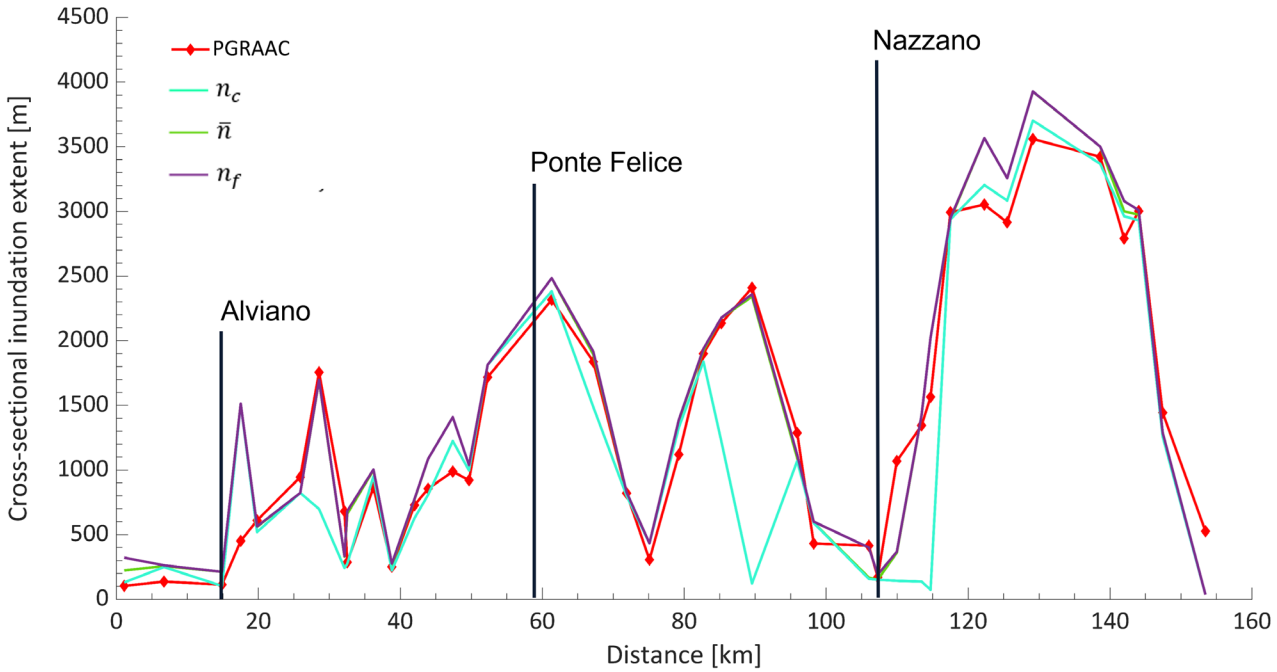

FIGURE 10 Cross-sectional inundation extent for 40 cross sections along the extracted network for different Manning's n values. Cross section position is identified with the diamonds on the red curve

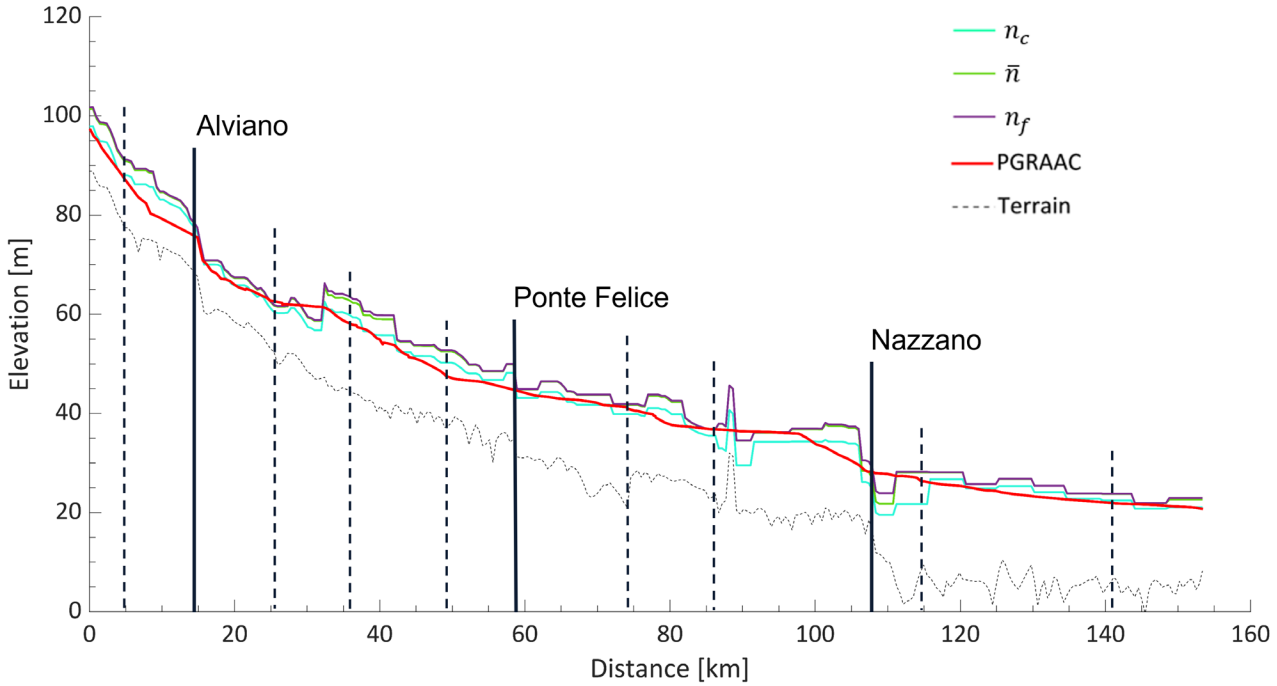

FIGURE 11 Water level profiles for $L = 5$ km channel segments, 2×2 m DTM resolution, and either the maximum and minimum value of the Manning coefficient, n_f and n_c. The terrain profile represents the elevation of the channel network extracted with the tool GeoNet from a 2×2 m DTM resolution. The location of the small dams is depicted with black lines, black-dashed vertical lines represent the location of the main bridges

et al. (2013), where an empirical conceptual algorithm was adopted for simulation on the same area, but using a coarse grid of 90 m. Consequently, some discrepancies due to the low level of detail provided are expected, especially at river junctions and in highly urbanized areas.

Channel segmentation length influences the entire process by affecting the accuracy of the synthetic rating curves. Channel hydraulic properties, such as cross-sectional area, wetted perimeter, slope, etc., of each stream reach are evaluated, through the HAND raster, taking the average of catchment characteristics for each segment. A small segmentation length produces better overall results in terms of inundation extent due to better representation of the local stage-discharge relationships; however, it provides water profiles that are more variable with respect to the reference one. A fair balance between these two contrasting requirements allows determining the optimum segmentation length. The latter is expected to be variable for each specific river portion, being generally affected by the river slope (Godbout et al., 2019). As a consequence, it might be recommended to perform different simulations with different segmentation lengths in different areas before fixing the parameter values.

Manning roughness coefficients also affect the model performance through the synthetic rating curves. GeoFlood applies an average value of the coefficient assuming it constant for each segment; consequently, it depends on the segment length and on the morphology of the region. In particular, in large valleys where the difference between the channel and the floodplain values can be significant, the floodplain value has a stronger impact on the average value and consequently on the rating curve; this is what happens in our case study. In the case of the Tiber River, we used Manning coefficient values for channel and floodplains that were calibrated for the standard hydrodynamic one-dimensional modeling approach by PGRAAC; the results suggest a better performance of GeoFlood for a Manning value smaller than that used by PGRAAC. Hence, whenever possible, the calibration of this parameter is highly recommended, taking advantage of GeoFlood's capability of performing simulations in short times.

Regarding the water level profiles, the discrepancy and the irregular behavior observed in the results mainly depend on the characteristics of the GeoFlood workflow, that is, the adoption of uniform conditions to solve for the water profile quickly, compared with the hydrodynamic reference solution. In addition, the effect of the slope, both low and steep, can be significant in the calculation of synthetic rating curves, producing depths that lead to over-estimation of the inundation extent and water level profile in low slope catchments, as also pointed out by Godbout et al. (2019).

As shown in our results, infrastructures, such as bridges, railways, and levees, appear not to affect the results, mainly in term of inundation extent. In terms of water

level profile, due to their irregular behavior, it is difficult to detect the effect of local infrastructures; more analysis might be required in order to cope with this aspect, for instance evaluating the backwater lengths along the river (Samuels, 1989). However, we noticed some discrepancy of the flood extent close to existing small dams. The over-estimation that occurs in the Alviano small dam area is due to the inaccuracy of GeoFlood in correspondence of reservoirs; while the under-estimation is mainly detected in areas characterized by a difference in altitude due to the presence of the dam structure that might have influenced the rating curves. In the HAND raster, infrastructures are detected as dry terrain (Figures 3, 6, and 9) if their elevation is higher than the depths extracted from the rating curves. However, infrastructures such as culverts are not accounted for in GeoFlood, unlike hydraulic models, and hydraulic continuity and regulation are not ensured, leading to possible under-estimation of flooding. This could affect in particular the scenarios corresponding to smaller return periods that we have not explored here. Hence, the effect depends on the type of structure as function of the return period, further requiring a more in-depth knowledge of the area as well as specific and technical information on the operation rules, which is not consistent with the general nature of Geoflood. The analysis of different return period scenarios could help further investigate the role of some of the parameters involved, in particular those controlling the stage-discharge relationship; for this reason, the analysis of different return period scenarios will be the subject of future work.

Despite a slight over-estimation of the inundation extent, which is also visible in water level profiles, the overall comparison of GeoFlood maps with that provided by PGRAAC is quite successful. In fact, despite the limitations discussed above, the results are rather robust in the case analyzed here, suggesting that the adoption of suboptimal parameter values does not affect much the results of the analysis. This is true especially if we take into account the large estimation uncertainty that characterizes flood mapping. As shown by Annis, Nardi et al. (2020), the estimation uncertainty of flood extent, water level, and velocity, is dominated by the uncertainty characterizing flood discharge estimates. Hence, the use of a detailed and costly hydrodynamic model, with a related intensive data acquisition (river sections, floodplain, levees, bridges and all the infrastructures present in the river), cannot help reducing the overall error, and the use of simplified methods already gives significant information for the delineation of preliminary flood maps, provided that geomorphologic information (DTM) is accurately checked for potential errors in reproducing riverbed profile and slope. Nevertheless, methods like GeoFlood cannot be considered as surrogate to hydrodynamic models but they can be useful during emergencies, and for post event analysis and land use planning, quickly pointing out the critical areas that require more detailed analysis. Furthermore, thanks to the limited cost of implementation, mainly related to computational time and the limited number of inputs parameters, GeoFlood could be a valuable tool for a probabilistic assessment of the flooding event, which generally relies on Monte Carlo approaches, thus requiring a very large number of simulations. We recall that GeoFlood requires as input the distribution of discharge along the river network, which needs to be known a-priori or previously computed out of the program.

6 | CONCLUSIONS

In this study, we assessed the applicability of the GeoFlood approach on the medium-lower portion of the Tiber River (Italy) for large-scale flood preparedness.

Flood maps were produced for a 200-year return period scenario and compared with the maps provided by the local authority (PGRAAC plan, 2013) based on standard detailed hydrodynamic modeling approaches. We performed a sensitivity analysis to explore the main parameters that might affect the results, both individually and combined, like DTM resolution, channel segment length, and Manning's roughness coefficient. The results are produced in terms of the overall inundation extent, cross-sectional inundation extent, and water level profile. A critical evaluation of GeoFlood potentials and limitations is summarized as follows.

- Flood maps produced with GeoFlood well reproduce that provided by the PGRAAC. The comparison is made by overlapping layers for each simulation obtaining a general over-estimation in term of inundation extent of the order of 5%. The corresponding water level profiles behave coherently, even if they are affected by the terrain elevation, and by the simplifications and uncertainties related to the methodology used in this work.
- The sensitivity analysis suggests optimal parameters values, namely DTM resolution and segment length, which could be adopted in other case studies of similar characteristics (e.g., shape and slope of the valley). Whenever possible, the Manning coefficient should be calibrated based on available observations.
- The sensitivity analysis also shows that the main parameters involved for the accurate estimation of inundation extent and water level profiles have a limited impact, confirming that GeoFlood produces robust results.
- Further, our results suggest that the effect of infrastructures is almost negligible when working on large

areas, apart from major hydraulic structures, such as dams, that alter the natural water profile even for small discharge values and based on regulation rules (which cannot be accounted for in GeoFlood).

All the aspects mentioned above make GeoFlood a valid framework for the approximation of inundation mapping over large scales for fluvial flooding assessment, also considering all the uncertainties involved in any mapping procedure. The tradeoff between limited costs, easiness of implementation, and overall accuracy makes GeoFlood and similar approaches useful tools that can provide valid information in support of more accurate but costly, fully fledged hydrodynamic models. Because of the limited use of resources, it is also a valuable tool for a preliminary delineation of regions where an investigation based on detailed hydrodynamic models is required.

ACKNOWLEDGMENTS

The authors would like to thank the Associate Editor and two anonymous Reviewers for the time spent on the manuscript and the comments provided that helped improve the manuscript. Claudia D'Angelo, Aldo Fiori, and Elena Volpi acknowledge funding from the Italian Ministry of Education, University and Research (MIUR), in the frame of the Departments of Excellence Initiative 2018–2022, attributed to the Department of Engineering of Roma Tre University, and the Italian Ministry of Environment, Land and Sea Protection (MATTM) through the project SimPRO. Also, this study was supported in part by NOAA (NA19OAR4590229) and by Planet Texas 2050, a research grand challenge initiative of The University of Texas at Austin.

DATA AVAILABILITY STATEMENT

The 2-meter Lidar-derived DTM is available upon request from the Italian Ministry of the Environment (MATTM) at http://www.pcn.minambiente.it/mattm/. The PGRAAC data that support the findings of this study are openly available at http://www.autoritadistrettoac.it.

ORCID


Elena Volpi https://orcid.org/0000-0002-9511-1496

REFERENCES

Alfieri, L., Salamon, P., Bianchi, A., Neal, J., Bates, P. D., & Feyen, L. (2014). Advances in pan-European flood hazard mapping. *Hydrological Processes*, *28*, 4067–4077.

Annis, A., & Nardi, F. (2021). GFPLAIN and multi-source data assimilation modeling: Conceptualization of a flood forecasting framework supported by hydrogeomorphic floodplain rapid mapping. *Hydrology*, *8*, 143.

Annis, A., Nardi, F., Morrison, R. R., & Castelli, F. (2019). Investigating hydrogeomorphic floodplain mapping performance with varying DTM resolution and stream order. *Hydrological Sciences Journal*, *64*(5), 525–538.

Annis, A., Nardi, F., Petroselli, A., Apollonio, C., Arcangeletti, E., Tauro, F., Belli, C., Bianconi, R., & Grimaldi, S. (2020). UAV-DEMs for small-scale flood hazard mapping. *Water*, *12*, 1717.

Annis, A., Nardi, F., Volpi, E., & Fiori, A. (2020). Quantifying the relative impact of hydrological and hydraulic modelling parameterizations on uncertainty of inundation maps. *Hydrological Sciences Journal*, *65*(4), 507–523.

Apel, H., Aronica, G. T., Kreibich, H., & Thieken, A. H. (2009). Flood risk assessments: How detailed do we need to be? *Natural Hazards*, *49*(1), 79–98.

Apel, H., Merz, B., & Thieken, A. H. (2008). Quantification of uncertainties in flood risk assessments. *International Journal of River Basin Management*, *6*, 149–162.

Apel, H., Thieken, A. H., Merz, B., & Blosch, G. (2004). Flood risk assessment and associated uncertainty. *Natural Hazards and Earth System Sciences*, *4*, 295–308.

Arrighi, C. & L. Campo (2019). Effects of digital terrain model uncertainties on high-resolution urban flood damage assessment. *Journal of Flood Risk Management*, *12*, (Suppl. 2):e12530, 1–12.

Bales, J. D., & Wagner, G. R. (2009). Sources of uncertainty in flood inundation maps. *Journal of Flood Risk Management*, *2*, 139–147.

Ball, T., Black, A., Ellis, R., Hemsley, L., Hollebrandse, F., Lardet, P., & Wicks, J. (2012). A new methodology to assess the benefits of flood warning. *Journal of Flood Risk Management*, *5*, 188–202.

Bates, P. D., Quinn, N., Sampson, C., Smith, A., Wing, O., Sosa, J., ... Krajewski, W. F. (2021). Combined modeling of US fluvial, pluvial, and coastal flood hazard under current and future climates. *Water Resources Research*, *57*(2), e2020WR028673.

Di Baldassarre, G., Nardi, F., Annis, A., Odongo, V., Rusca, M., & Grimaldi, S. (2020). Brief communication: Comparing hydrological and hydrogeomorphic paradigms for global flood hazard mapping. *Natural Hazards and Earth System Sciences*, *20*, 1415–1419.

Dottori, F., Salamon, P., Bianchi, A., Alfieri, L., Hirpa, F. A., & Feyen, L. (2016). Development and evaluation of a framework for global flood hazard mapping. *Advances in Water Resources*, *94*, 87–102.

Godbout, L., Zheng, J. Y., Dey, S., Eyelade, D., Maidment, D., & Passalacqua, P. (2019). Error assessment for height above the nearest drainage inundation mapping. *Journal of the American Water Resources Association*, *55*(4), 952–963.

Horrit, M. S., & Bates, P. D. (2001). Effects of spatial resolution on a raster-based model of flood flow. *Journal of Hydrology*, *253*, 239–249.

Koivumaki, L., Ahlo, P., Lotsari, E., Kayhko, J., Saari, A., & Hyyppa, H. (2010). Uncertainties in flood risk mapping: A case study on estimating building damages for a river flood in Finland. *Journal of Flood Risk Management*, *3*, 166–183.

Komolafe, A. A., Herat, S., & Avtar, R. (2018). Sensitivity of flood damage estimation to spatial resolution. *Journal of Flood Risk Management*, *11*, S370–S381.

Lhomme, J., P. Sayers, B. Gouldby, P. Samuels, M. Wills, & J. Mulet-Marti (2008). Recent development and application of a rapid flood spreading method. Proceedings of the European Conference on Flood Risk Management Research into Practice.

Manfreda, S., Di Leo, M., & Sole, A. (2011). Detection of flood-prone areas using digital elevation models. *Journal of Hydrologic Engineering*, *16*(10), 781–790.

Manfreda, S., Nardi, F., Samela, C., Grimaldi, S., Taramasso, A. C., Roth, G., & Sole, A. (2014). Investigation on the use of geomorphic approaches for the delineation of flood prone areas. *Journal of Hydrology*, *517*, 863–876.

Manfreda, S. & C. Samela (2019). A digital elevation model-based method for a rapid estimation of flood inundation depth. *Journal of Flood Risk Management*, *12* (Suppl. 1):e12541, 1–10.

Nardi, F., Biscarini, C., Di Francesco, S., Manciola, P., & Ubertini, L. (2013). Comparing a large-scale DEM-based floodplain delineation algorithm with standard flood maps: The Tiber River basin case study. *Irrigation and Drainage*, *62*(Suppl. 2), 11–19.

Nardi, F., Vivoni, E. R., & Grimaldi, S. (2006). Investigating a floodplain scaling relation using a hydrogeomorphic delineation method. *Water Resources Research*, *42*(9), W09409.

Nobre, A. D., Cuartas, L. A., Hodnett, M., Rennò, C. D., Rodrigues, G., Silveira, A., Waterloo, M., & Saleska, S. (2011). Height above the nearest drainage: A hydrologically relevant new terrain model. *Journal of Hydrology*, *404*, 13–29.

Nobre, A. D., Cuartas, L. A., Momo, M. R., Severo, D. C., Pinheiro, A., & Nobre, C. A. (2015). HAND contour: A new proxy predictor of inundation extent. *Hydrological Processes*, *30*, 320–333.

Pappenberger, F., Dutra, E., Wetterhall, F., & Cloke, H. L. (2012). Deriving global flood hazard maps of fluvial floods through a physical model cascade. *Hydrology and Earth System Sciences*, *16*(11), 4143–4156.

Passalacqua, P., Do Trung, D., Foufoula-Georgiou, E., Sapiro, G., & Dietrich, W. E. (2010). A geometric framework for channel network extraction from lidar: Nonlinear diffusion and geodesic paths. *Journal of Geophysical Research*, *115*, F01002.

Pena, F., & Nardi, F. (2018). Floodplain terrain analysis for coarse resolution 2D flood modeling. *Hydrology*, *5*(52), 1–16.

Petroselli, A. (2012). LIDAR data and hydrological applications at the basin scale. *GIScience & Remote Sensing*, *49*(1), 139–162.

Samela, C., Albano, R., Sole, A., & Manfreda, S. (2018). A GIS tool for cost-effective delineation of flood-prone areas. *Computers, Environment and Urban Systems*, *70*, 43–52.

Samela, C., Manfreda, S., De Paola, F., Giugni, M., Sole, A., & Fiorentino, M. (2016). DEM-based approaches for the delineation of flood-prone areas in an ungauged basin in Africa. *Journal of Hydrologic Engineering*, *21*(2), 06015010.

Sampson, C. C., Smith, A. M., Bates, P. D., Neal, J. C., Alfieri, L., & Freer, E. J. (2015). A high-resolution global flood hazard model. *Water Resources Research*, *51*, 7358–7381.

Samuels, P. G. (1989). Backwater lengths for rivers. *Proceedings of the Institution of Civil Engineers (London)*, *87*(Pt 2), 571–582.

Sangireddy, H., Stark, C. P., Kladzyk, A., & Passalacqua, P. (2016). GeoNet: An open-source software for the automatic and objective extraction of channel heads, channel network, and channel morphology from high resolution topography data. *Environmental Modelling & Software*, *83*, 58–73.

Savage, J. T. S., Pianosi, F., Bates, P. D., Freer, J., & Waganer, T. (2016). Quantifying the importance of spatial resolution and other factors through global sensitivity analysis of a flood inundation model. *Water Resources Research*, *52*, 9146–9163.

Schumann, G. J. P., Neal, J. C., Voisin, N., Andreadis, K. M., Pappenberger, F., Phan-thuwongpakdee, N., Hall, A. C., & Bates, P. D. (2013). A first large-scale flood inundation forecasting model. *Water Resources Research*, *49*, 6248–6257.

Teng, J., Jakeman, A. J., Vaze, J., Croke, D., Dutta, B. F. W., & Kim, S. (2017). Flood inundation modelling: A review of methods, recent advances and uncertainty analysis. *Environmental Modelling & Software*, *90*, 201–216.

Teng, J., Vaze, J., Dutta, D., & Marvanek, S. (2015). Rapid inundation modelling in large floodplains using LiDAR DEM. *Water Resources Management*, *29*, 2619–2636.

Tyrna, B., Assmann, A., Fritsch, K., & Johann, C. (2018). Large-scale high-resolution pluvial flood hazard mapping using the raster-based hydrodynamic two-dimensional model FloodAreaHPC. *Journal of Flood Risk Management*, *11*, S1024–S1037.

USACE (2016). *HEC RAS River Analysis system 2D modeling User's Manual. Version 5.0*. Institute for Water Resources Hydrologic Engineering Center HEC, Davis CA: CPD-68A.

van Alphen, J., Martini, F., Loat, R., Slomp, R., & Passchier, R. (2009). Flood risk mapping in Europe, experiences and best practices. *Journal of Flood Risk Management*, *2*, 285–292.

Vorogushyn, S., Bates, P. D., de Bruijn, K., Castellarin, A., Kreibich, H., Priest, S., Schröter, K., Bagli, S., Blöschl, G., Domeneghetti, A., Gouldby, B., Klijn, F., Lammersen, R., Neal, J. C., Ridder, N., Terink, W., Viavattene, C., Viglione, A., Zanardo, S., & Merz, B. (2018). Evolutionary leap in large-scale flood risk assessment needed. *WIREs Water*, *5*(e1266), 1–7.

Wing, O. E. J., Bates, P. D., Sampson, C. C., Smith, A. M., Johnson, K. A., & Erickson, T. A. (2017). Validation of a 30 m resolution flood hazard model of the conterminous United States. *Water Resources Research*, *53*, 7968–7986.

Winsemius, H. C., Van Beek, L. P. H., Jongman, B., Ward, P. J., & Bouwman, A. (2013). A framework for global river flood risk assessments. *Hydrology and Earth System Sciences*, *17*, 1871–1892.

Zheng, X., Maidment, D. R., Tarboton, D. G., Liu, Y. Y., & Passalacqua, P. (2018). GeoFlood: Large-scale flood inundation mapping based on high-resolution terrain analysis. *Water Resources Research*, *54*, 10013–10033.

Zheng, X., Tarboton, D. G., Maidment, D. R., Liu, Y. Y., & Passalacqua, P. (2018). River channel geometry and rating curve estimation using height above the nearest drainage. *Journal of the American Water Resources Association*, *54*(4), 785–806.

How to cite this article: D'Angelo, C., Passalacqua, P., Fiori, A., & Volpi, E. (2022). Identification of flood-prone areas with GeoFlood: Lessons learned from the Tiber River case study. *Journal of Flood Risk Management*, *15*(2), e12795. https://doi.org/10.1111/jfr3.12795